A LogTV Nonconvex Regularization Model for Magnetic Resonance Imaging

Lirong Wang , Sayang Mohd Deni, and Zalina Zahid

***Abstract*—Magnetic resonance imaging (MRI) is one of the essential elements in medical areas, particularly in diagnostic procedures. However, due to the under-sampling process, the reconstructed MR image leads to incomplete output, including the edge being blurred and the noise remaining, which are considered fundamental problems of MRI analysis and the diagnosis procedure. The total variational (TV) regularization technique is a standard method for MRI reconstruction. This paper proposes a nonconvex regularization MRI model (LogTV) to construct a logarithm penalty function that could effectively prevent the system due to underestimating characteristics. Moreover, this study will offer an improved alternating direction method of multipliers (ADMM) algorithm and the algorithm's convergence in solving the new nonconvex model. Finally, the numerical proposed model is expected to have a better effect on MRI than similar models. That is, the value of the peak signal-to-noise ratio (PSNR) is more significant, the relative error (RE) is minor, and the structural similarity index measurement (SSIM) is closer to 1 under the proposed model.**

***Index Terms*—MRI reconstruction, LogTV regularization, DC decomposition, ADMM**

I. INTRODUCTION

IT is known that MRI mainly relies on gradient magnetic field and RF pulse to image tissue. With its excellent performance, MRI occupies a pivotal position in modern medicine [1]. However, the inherent time-consuming problem of signal acquisition seriously limits the application of MRI technology in clinical diagnosis. On the one hand, this defect will bring discomfort to the tested patients and the inevitable body movement, including heartbeat and gastrointestinal peristalsis. Thus, this scenario will form motion artifacts in the MR image, introduce noise and reduce the imaging quality, which is very unfavorable for doctors to produce accurate lesion information from the MR image and even lead to misdiagnosis or missed diagnosis. On the other hand, low inspection efficiency will make expensive inspection costs, which limits its further promotion and applications. Therefore, the focus and difficulty of MRI research have been eliminating redundancy, improving MRI acquisition efficiency, speeding up signal acquisition, shortening imaging time, reducing patient discomfort, accurately restoring images, and improving diagnostic rate [1].

Compressed sensing (CS) [2-3] the theory can reconstruct MRI images with a small amount of data and achieve good reconstruction results by using the sparsity of image data [4-5]. In MRI combined with CS theory, constructing constraint terms using the sparsity of images in a specific transform domain is the most commonly used. In addition, TV regularization also is popular with sparse regularization, which is very effective in solving the problem of image smoothing under noise [6]. It not only effectively suppresses the noise but also in preserving the details, such as the texture and edge of the image. Therefore, it is widely used in signal processing, image denoising, image reconstruction, and other fields [7-9]. The MRI method gradually develops based on the total variation (TV) regularization transform.

The MRI images can be abstracted as underdetermined linear models

$$y = Ax + \varepsilon, \tag{1.1}$$

where $x \in R^n$ is the MRI to be reconstructed, $\boldsymbol{\varepsilon}$ is the noise, $y \in R^m$ represents the K -space signal under-sampled by the nuclear magnetic resonance coil, and its dimension is far lower than $\boldsymbol{x}$. $A = P \times F$, $P \in R^{m \times n}$ is the incomplete sampling template, and the standard sampling template has radial sampling, random sampling, Cartesian sampling, and so on. $F \in R^{n \times n}$ is a sparse Fourier transform operator. MRI reconstruction aims to recover $\boldsymbol{x}$ from $\boldsymbol{y}$ according to the model (1.1). In general, the simplest way to solve an underdetermined equation (1.1) is to use ordinary least squares estimation (OLSE), which is based on the maximum likelihood estimation of statistics. However, the least square method can not produce a simple model and cannot feature or variable selection, so the effect of model prediction and interpretability is inferior. In MRI problems, the dimension of sampled data is much smaller than that of accurate data. OLSE is usually an underdetermined system or an ill-conditioned issue. Therefore, we must use the regularization technique to solve the sparse optimization problem and get a suitable solution. MRI reconstruction techniques based on CS often employ the TV or generalized TV form as a convex regularization term to improve the sparsity in gradient space. And the standard TV model is

Manuscript received September 19, 2022; revised April 19, 2023

This work was supported in part by the Scientific Research Fund of Hunan Provincial Education Department 20A273 and the Research Fund of Mathematics Discipline of Hunan University of Humanities, Science and Technology 2020SXJJ01.

Lirong Wang is a lecturer of School of Mathematics and Finance, Hunan University of Humanities, Science and Technology, Loudi, 417000, P.R.China and she is slso a postgraduate student of Faculty of Computer and Mathematical Sciences, Universiti Teknologi MARA (UiTM), UiTM Shah Alam, 40450 Selangor, Malaysia, (e-mail: ldwlr1234@163.com).

Sayang Mohd Deni is a Professor of Faculty of Computer and Mathematical Sciences，Universiti Teknologi MARA (UiTM), UiTM Shah Alam, 40450 Selangor, Malaysia. (e-mail: sayan929@uitm.edu.my).

Zalina Zahid is a Doctor of Faculty of Computer and Mathematical Sciences，Universiti Teknologi MARA (UiTM), UiTM Shah Alam, 40450 Selangor, Malaysia. (e-mail: zalin405@uitm.edu.my).

reconstructed as described below:

$$\min_x \frac{1}{2}\| y - Ax \|_2^2 + \lambda \| x \|_{\mathrm{TV}}, \qquad (1.2)$$

where $\|x\|_{\mathrm{TV}}$ is the regularization term, actually means $\| Dx \|_1$ ($\boldsymbol{D}$ is gradient operator), and $\lambda > 0$ is called the regularization parameter. Classical TV regularization is convex, which involves $L_1 = \|\cdot\|_1$ norm regularization [3,6,10]. However, L_1 the norm is not differentiable and will underestimate the larger value in the sparse solution, producing a biased estimate. The $L_p = \|\cdot\|_p (0 < p < 1)$ norm is used as the regularization term to estimate the more significant value in the sparse solution more effectively [11]. However, because the objective function itself is nonconvex, the solution process is often complicated, which will fall into the optimal local value. To overcome the shortcomings of the L_1 and L_p regularization, some nonconvex regularization methods are proposed based on minimax-concave (MC), smoothly clipped absolute deviation (SCAD), arctangent (Atan) penalty functions, etc.

For example, Liu et al. [12] introduced MCTV regularization terms with MC penalty function, and later Shen et al. [13] constructed a novel MRI reconstruction model (MCTV- L2) via L2 norm and MC penalty. Mehranian et al. [14] and Luo et al. [15] introduced nonconvex SCAD regularization for MRI or image denoising to improve the performance of TV regularizations. Luo et al. [16] constructed a nonconvex reconstruction model of MRI using the arctangent function. In the document, Zhang et al. built a new TV-Log nonconvex model for impulse noise denoising [17]. Wang et al. considered introducing a logarithmic transformation method to solve linear multiplicative programming to improve the model [18].

Inspired by the above papers, in this paper, a Log penalty function is used to replace the TV regularization term since the Log penalty function also can overcome the over-penalization associated with the norm. This LogTV model can be written as

$$\min_x \frac{1}{2}\| y - Ax \|_2^2 + \lambda \| x \|_{\mathrm{LogTV}}, \qquad (1.3)$$

where

$$\| x \|_{\mathrm{LogTV}} \triangleq \Phi_\gamma(Dx) = \sum_{i=1}^{n} \frac{1}{\gamma} \mathrm{Log}(1 + \gamma \| D_i x \|_1),$$

for more details, please see Section 2.

In the sparse reconstruction problem, an efficient sparse reconstruction algorithm is the key to ensuring the wide application of sparse reconstruction, and many algorithms have been developed [19]. The ADMM is a simple and effective convex optimization algorithm [20]. In essence, it is a particular operator-splitting method. Its main idea is to transform unconstrained optimization problems into constrained problems by splitting variables and then solving them alternately, which is fast and easy to program. The algorithm is widely used to solve high-dimensional and complex sparse optimization models [13,20-25]. Based on the advantages of this algorithm, this paper also considers using ADMM to solve the newly proposed model.

This study focuses on the reconstruction model and algorithm of MRI, which includes enhancing the nonconvex MRI model to a higher degree, solving the LogTV model by using an improved ADMM algorithm and verifying the proposed algorithm through simulation and benchmark data. Hence, the study is conducted and structured as follows. The study design of this research is given in Figure 1, and the explanation of the nonconvex LogTV MRI reconstruction model is presented in Section 2. In the next section, the improvement of the ADMM algorithm for solving the nonconvex model is proposed. This is followed by Section 4, where the analysis of convergence and its algorithm is explained. In section 5, some experiments verify the effectiveness of the new nonconvex model. Finally, some conclusions are provided at the end of this manuscript.

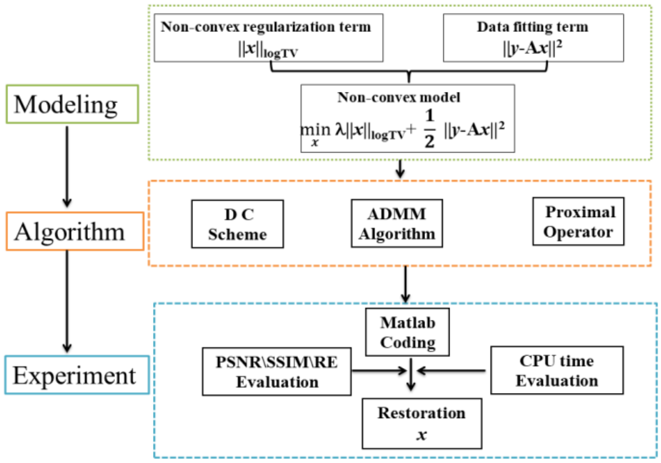

Fig. 1. The demonstration of the study design of this paper.

II. LOGTV MRI MODEL

This section defines the Log-TV regularization term via a Log-penalty function. The interpretation of the new non-convex regularization model for MRI reconstruction is as follows.

Firstly, some properties of the Log function are shown, and let

$$\phi_\gamma(s) = \frac{1}{\gamma} \mathrm{Log}(1 + \gamma |s|), \quad s \in R \qquad (2.1)$$

According to the definition of the function $\phi_\gamma(s)$, in R^+, the function $\phi_\gamma(s)$ is continuously differentiable and concave. Then, another function $\psi_\gamma(s)$ is considered that is induced by

$$\psi_\gamma(s) = |s| - \phi_\gamma(s), \quad \gamma > 0. \qquad (2.2)$$

It is observed that $\psi_\gamma(s)$ is continuously differentiable and convex in $\boldsymbol{R}^+$. Figure 2 shows the curve of functions $\phi_\gamma(s)$ and $\psi_\gamma(s)$, from which the estimation $\phi_\gamma(s)$ is obtained, which is suitable for fitting $|s|_0$ than $|s|_1$.

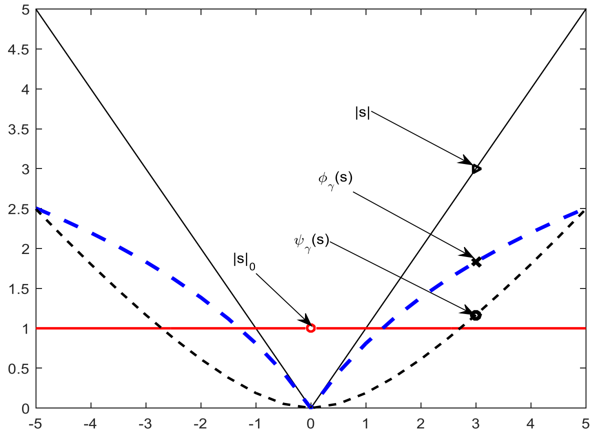

Fig.2. Illustration of functions $|s|_0$, $|s|$, $\phi_\gamma(s)$, $\psi_\gamma(s)$

The multivariate generalization of function $\psi_\gamma(s)$ and set $\Psi_\gamma : R^n \to R$ is given as follows

$$\Psi_\gamma(\boldsymbol{v}) = \sum_{i=1}^{n} \psi_\gamma(\boldsymbol{v}_i), \quad \boldsymbol{v} \in \boldsymbol{R^n}, \quad \gamma > 0. \tag{2.3}$$

From [26-27], the following multivariate functions are defined

$$\Phi_\gamma(\boldsymbol{v}) = \| \boldsymbol{v} \|_1 - \Psi_\gamma(\boldsymbol{v}), \quad \boldsymbol{v} \in \boldsymbol{R^n} \tag{2.4}$$

By replacing $\boldsymbol{v}$ by Dx in Equation 2.4, the following LogTV regularization definition is obtained.

Definition 2.1. The nonconvex LogTV regularization:

$$\|x\|_{\mathrm{LogTV}} = \Phi_\gamma(Dx) = \| Dx \|_1 - \Psi_\gamma(Dx). \tag{2.5}$$

Now, we consider the following LogTV model to replace the traditional TV model in MRI reconstruction

$$\min_x \lambda \| x \|_{\mathrm{LogTV}} + \frac{1}{2} \| y - Ax \|_2^2 . \tag{2.6}$$

where $\lambda > 0$ and $\|x\|_{\mathrm{LogTV}}$: $R^n \to R$ is given by the formula (2.5). Since the function $\phi_\gamma(s)$ is nonconvex, the model (2.6) is nonconvex.

Lemma 2.1. Let $E : R^n \to R$ be the function

$$E(x) = \lambda \| x \|_{\mathrm{LogTV}} + \frac{1}{2} \| y - Ax \|_2^2 \tag{2.7}$$

where $\lambda > 0$ and $\|x\|_{\mathrm{LogTV}}$: $R^n \to R$ is given by (2.5). If the parameter $\gamma > 0$ such that $\lambda\gamma D^T D \preceq A^T A$ then $E(x)$ is convex.

Proof: Firstly, from (2.7) and (2.5), we have

$$\begin{aligned} E(x) &= \lambda \| x \|_{\mathrm{LogTV}} + \frac{1}{2} \| y - Ax \|_2^2 \\ &= \lambda \Phi_\gamma(Dx) + \frac{1}{2}\left[\| y \|_2^2 + \| Ax \|_2^2 - 2y^T Ax \right] \\ &= \left[\lambda \| Dx \|_1 + \frac{1}{2} \| Ax \|_2^2 - y^T Ax \right] + \left[\frac{1}{2} \| Ax \|_2^2 - \lambda \Psi_\gamma(Dx) \right]. \end{aligned}$$

Then, the function E is convex if the last term $[\bullet]$ is convex.

Hence, we define $\tilde{G} : R^n \to R$ it as

$$\tilde{G}(x) = \frac{1}{2} \| Ax \|_2^2 - \lambda \Psi_\gamma(Dx). \tag{2.8}$$

Now, we show the function $\tilde{G}$ is convex and rewrite $\tilde{G}$ it as

$$\tilde{G}(x) = \underbrace{\frac{1}{2}\left(\| Ax \|_2^2 - \lambda\gamma \| Dx \|_2^2 \right)}_{G_1(x)} + \underbrace{\lambda \left(\frac{\gamma}{2} \| Dx \|_2^2 - \Psi_\gamma(Dx) \right)}_{G_2(x)} . \tag{2.9}$$

Since $\lambda\gamma D^T D \preceq A^T A$ is given, it is evident that $G_1(x)$ is convex. For the function $G_2(x)$, we can prove that it is a convex function by referring to Proposition 1 in [27]. Hence, the lemma is true.

III. PROPOSED ALGORITHM

This section presents the proposed solution algorithm of the model (2.6). Firstly, the reformulation of the model from Equation (2.7) is displayed below

$$\begin{aligned} E(x) &= \lambda \| x \|_{\mathrm{LogTV}} + \frac{1}{2} \| y - Ax \|_2^2 \\ &= \lambda \Phi_\gamma(Dx) + \frac{1}{2} \| y - Ax \|_2^2 . \end{aligned} \tag{3.1}$$

Due to the existence of nonconvex functions, it is difficult to solve the problem (3.1). Inspired by reference [28], our strategy is decomposing the equation into the difference of convex (DC) components, i.e. $E(x) = G(x) - H(x)$, where

$$\begin{cases} G(x) = \frac{1}{2} \| y - Ax \|_2^2 + c \| x \|_2^2 + \sum_{i=1}^{n} \| D_i x \|_2 \\ H(x) = c \| x \|_2^2 + \sum_{i=1}^{n} \| D_i x \|_2 - \lambda \Phi_\gamma(Dx) \end{cases}$$

The $G(x) - H(x)$ called DC decomposition of the function $E(x)$ and $\boldsymbol{c} > 0$ is a parameter. To ensure that functions $G(x)$ and $H(x)$ are strongly convex, this study will propose the appropriate estimation by considering limiting the parameter c to the function. In the design of the DC algorithm, consider the following two sequence iterations $\{ d^k \}$ and $\{ x^k \}$,

$$\begin{cases} d^k \in \partial H(x^k) \\ x^{k+1} = \arg\min_x J(x, x^k) = \arg\min_x G(x) - (H(x^k) + \langle d^k, x - x^k \rangle) \end{cases} \tag{3.2}$$

For the sequence $\{x^k\}$,

$$\begin{aligned} x^{k+1} = \arg\min_x & \frac{1}{2} \| y - Ax \|_2^2 + c \| x \|_2^2 \\ & - 2c\langle x^k, x \rangle + \sum_{i=1}^{n} \left(\| D_i x \|_2 - \lambda \langle D_i x, f_i^k q_i^k \rangle \right) \end{aligned} \tag{3.3}$$

where $f_i^k = \dfrac{\gamma \| D_i x^k \|_2}{1 + \gamma \| D_i x^k \|_2}, q_i^k = \dfrac{D_i x^k}{\| D_i x^k \|_2}$. Note that, if $\| D_i x^k \|_2 = 0$, then $q_i^k = 0$. In fact,

$$\langle d^k, x \rangle - 2c \langle x^k, x \rangle = \sum_{i=1}^{n} \langle D_i x, \lambda f_i^k q_i^k \rangle.$$

In solving the problem that arises in Equation (3.3), the auxiliary variables $z = Dx$ are introduced, and rewrite the equation as follows

$$\begin{aligned} &\min_{x, z_i} \frac{1}{2} \| y - Ax \|_2^2 + c \| x \|_2^2 - 2c \langle x^k, x \rangle + \sum_{i=1}^{n} \left(\| z_i \|_2 - \langle z_i, \lambda f_i^k q_i^k \rangle \right), \\ &s.t. \quad z_i = D_i x \end{aligned} \tag{3.4}$$

The corresponding augmented Lagrangian function of (3.4) is given by

$$L(z,x,w)=\frac{1}{2}\| y-Ax\|_2^2+c\| x\|_2^2-2c\langle x^k,x\rangle+\sum_{i=1}^{n}\left(\| z_i\|_2-\langle z_i,\lambda f^k q^k\rangle-\langle w_i,z_i-D_ix\rangle+\frac{\beta}{2}\| z_i-D_ix^k\|_2^2\right), \tag{3.5}$$

where w_i is the Lagrangian multiplier. The classical ADMM framework (3.5) includes the following steps:

- step1. z –Subproblem update

$$z^{k+1}=\arg\min_z\sum_{i=1}^{n}\left(\| z_i\|_2-\langle z_i,\lambda f_i^k q_i^k\rangle-\langle w_i^k,z_i-D_ix^k\rangle+\frac{\beta}{2}\| z_i-D_ix^k\|_2^2\right) \tag{3.6}$$

- step2. x –Subproblem update

$$x^{k+1}=\arg\min_x\frac{1}{2}\| y-Ax\|_2^2+c\| x\|_2^2-2c\langle x^k,x\rangle+\sum_{i=1}^{n}\left(\langle w_i^k,D_ix\rangle+\frac{\beta}{2}\| z_i^{k+1}-D_ix\|_2^2\right) \tag{3.7}$$

- step3. w – update

$$w^{k+1}=w_i^k-\beta\delta(z_i^{k+1}-D_ix^{k+1}) \tag{3.8}$$

where $\delta\in(0,\frac{1+\sqrt{5}}{2})$ is the step size.

For the z-Subproblem (3.6), reference [22,23] has the closed-form solution as

$$z_i^{k+1}=\max\left\{\| D_ix^k+\frac{w_i^k+\lambda f_i^k q_i^k}{\beta}\|_2-\frac{1}{\beta},0\right\}\frac{D_ix^k+\frac{w_i^k+\lambda f_i^k q_i^k}{\beta}}{\| D_ix^k+\frac{w_i^k+\lambda f_i^k q_i^k}{\beta}\|_2}. \tag{3.9}$$

For the x -subproblem (3.7), its closed-form solution is

$$x^{k+1}=\left(\sum_{i=1}^{n}\beta D_i^TD_i+A^TA+2cI\right)^{-1}\left(\sum_{i=1}^{n}(\beta D_i^Tz_i^{k+1}-D_i^Tw_i^k)+A^Tb+2cx^k\right) \tag{3.10}$$

It is quite complicated to calculate (3.10) directly due to the computational complexity of the inverse matrix is $O(n^3)$. To simplify the calculation of the subproblem (3.7), the linearization approximation technique will be used as

$$\frac{1}{2}\| y-Ax\|_2^2\approx\frac{1}{2}\| Ax^k-y\|_2^2+\langle A^TAx^k-A^Ty,x-x^k\rangle+\frac{1}{2\tau}\| x-x^k\|_2^2 \tag{3.11}$$

Applying the above formula to (3.7), the following result will be produced

$$x^{k+1}=\arg\min_x\frac{1}{2}\| Ax^k-y\|_2^2+\langle A^TAx^k-A^Ty,x-x^k\rangle+\frac{1}{2\tau}\| x-x^k\|_2^2+c\| x\|_2^2-2c\langle x^k,x\rangle+\sum_{i=1}^{n}\left(\langle w_i^k,D_ix\rangle+\frac{\beta}{2}\| z_i^{k+1}-D_ix\|_2^2\right). \tag{3.12}$$

By considering the first-order optimality condition of (3.12), it follows that

$$x^{k+1}=\left(D^TD+\frac{1+2c\tau}{\beta\tau}I\right)^{-1}\left(D^T\left(z_i^{k+1}-\frac{w_i^k}{\beta}\right)+\frac{1+2c\tau}{\beta\tau}x^k-\frac{1}{\tau}A^T(Ax^k-y)\right), \tag{3.13}$$

where I is an identity matrix. Ref [26] points out that equation (3.13) can be effectively solved by fast Fourier transform (FFT). Now, the specific algorithm steps are given,

---

Algorithm LogTV

Initialization: Given A,b, **Select** $\lambda,\ \gamma,\ c,\ \tau,\ \delta,\ \beta,\ \varepsilon_0,\ N_{iter}$.

Initialize x^0, w^0 .

Main iteration loop:

for $k=1,2,...,N_{\max}$ do

 z - updating:

 compute z^{k+1} by using (3.9).

 x- updating:

 compute x^{k+1} by using (3.13) .

 w- updating:

 $w_i^{k+1}=w_i^k-\beta\delta(z_i^{k+1}-D_ix^{k+1})$

 Exit criterion:

 $\varepsilon^{k+1}=\frac{\| x^{k+1}-x^k\|_2}{\| x^k\|_2}$

 if $\varepsilon^{k+1}<\varepsilon_0$ then

  exit

 end

end

where $N_{\max}$ represents the maximum number of iterations.

Note: According to the proximal operator definition

$$\operatorname{prox}_{\lambda f}(x)=\arg\min_u\frac{\| x-u\|_2^2}{2\lambda}+f(u),$$

set

$$P_1=\| z_i\|_2,\ P_2=\sum_{i=1}^{n}\left(\langle w_i^k,D_ix\rangle+\frac{\beta}{2}\| z_i^{k+1}-D_ix\|_2^2\right),$$

the LogTV method solution (3.5) can be regarded as a proximity operator. And the $z-$ subproblem (3.6) and $x-$ subproblem (3.12) can be formulated as

$$z_i^{k+1}=\operatorname{prox}_{\frac{1}{\beta}P_1}\left(D_ix^k+\frac{w_i^k+\lambda f_i^k q_i^k}{\beta}\right), \tag{3.14}$$

$$x^{k+1}=\operatorname{prox}_{\frac{\tau}{1+2c\tau}P_2}\left(x^k-\frac{\tau}{1+2c\tau}A^T(Ax^k-y)\right), \tag{3.15}$$

respectively.

IV. CONVERGENCE ANALYSIS

This section demonstrates the analysis of the convergence of the sequence $\{x^k\}$, which is obtained by the LogTV algorithm. Furthermore, to ensure the convergence of the LogTV method, the limiting conditions of parameter selection are proposed.

Proposition 4.1. If $0<\tau<\frac{1}{w_{\max}(A^TA)}$, the sequence of the LogTV method satisfies

$$L(z^{k+1},x^{k+1},w^k)\le L(z^{k+1},x^k,w^k),$$

where $w_{\max}(A^TA)$ is the Lipschitz constant.

Proof. For any $x\in R^n$, the Hesse matrix of quadratic term

$\frac{1}{2}\|\boldsymbol{y}-\boldsymbol{Ax}\|_2^2$ satisfies the Lipschitz condition, and the following result will be obtained

$$\begin{aligned}\frac{1}{2}\|\boldsymbol{y}-\boldsymbol{Ax}\|_2^2 &\leq \frac{1}{2}\|\boldsymbol{y}-\boldsymbol{Ax^k}\|_2^2 \\ &+\left\langle \boldsymbol{A^TAx^k}-\boldsymbol{A^Ty},\boldsymbol{x}-\boldsymbol{x^k}\right\rangle+\frac{\boldsymbol{w_{\max}(A^TA)}}{2}\|\boldsymbol{x}-\boldsymbol{x^k}\|_2^2,\end{aligned} \tag{4.1}$$

Let

$$P(x)=c\|x\|_2^2-2\left\langle x^k,x\right\rangle+\sum_{i=1}^n\left(\left\langle w_i^k,D_ix\right\rangle+\frac{\beta}{2}\|z_i^{k+1}-D_ix\|_2^2\right),$$

thus

$$\begin{aligned}x^{k+1}&=\arg\min_x\frac{1}{2}\|Ax^k-y\|_2^2 \\ &+\left\langle A^TAx^k-A^Ty,x-x^k\right\rangle+\frac{1}{2\tau}\|x-x^k\|_2^2+P(x).\end{aligned} \tag{4.2}$$

By comparing (4.2) with (3.7), combined with formula (4.1) and x^{k+1} is the minimum of (4.2), the following inequality will be produced

$$\begin{aligned}&\frac{1}{2}\|Ax^{k+1}-y\|_2^2+P(x^{k+1})\leq\frac{1}{2}\|Ax^k-y\|_2^2 \\ &+\left\langle A^TAx^k-A^Ty,x^{k+1}-x^k\right\rangle+\frac{w_{\max}(A^TA)}{2}\|x^{k+1}-x^k\|_2^2+P(x^{k+1}) \\ &\leq\frac{1}{2}\|Ax^k-y\|_2^2+P(x^k)-\frac{1}{2}\left(\frac{1}{\tau}-w_{\max}(A^TA)\right)\|x^{k+1}-x^k\|_2^2.\end{aligned} \tag{4.3}$$

Then, comparing (4.2) with (3.11), thus

$$L(z^{k+1},x^{k+1},w^k)\leq L(z^{k+1},x^k,w^k)-\frac{1}{2}\left(\frac{1}{\tau}-w_{\max}(A^TA)\right)\|x^{k+1}-x^k\|_2^2$$

the result holds.

Based on Proposition 4.1, where the parameter satisfies certain conditions, the solution generated from the LogTV method showed descending direction of the *x*-subproblem.

Theorem 4.1. Assume that the parameter τ satisfies Proposition 4.1, then the sequence $\{x^k\}$ generated from the LogTV method satisfies $\lim_{k\to\infty}\|x^{k+1}-x^k\|_2=0$.

Proof. To prove the theorem's conclusion, we first analyze that the sequence $\{E(x^k)\}$ is monotonically decreasing and the sequence $\{x^k\}$ is bounded.

Firstly, from the definition of function $E(x)$ in (3.7), the following function is obtained

$$\begin{aligned}E(x^k)-E(x^{k+1})&=\frac{1}{2}\|Ax^k-y\|_2^2-\frac{1}{2}\|Ax^{k+1}-y\|_2^2 \\ &+\lambda\sum_{i=1}^n\left(\phi_\gamma(\|D_ix^k\|_2)-\phi_\gamma(\|D_ix^{k+1}\|_2)\right)\end{aligned}$$

As $\boldsymbol{x^{k+1}}$ is the iterative solution of the ADMM framework (3.6-3.8) for the sub-problem (3.5), then

$$\begin{aligned}&\frac{1}{2}\|Ax^{k+1}-y\|_2^2+c\|x^{k+1}\|_2^2-\left\langle d^k,x^{k+1}-x^k\right\rangle+\lambda\sum_{i=1}^n\left(\|D_ix^{k+1}\|_2\right) \\ &\leq\frac{1}{2}\|Ax^k-y\|_2^2+c\|x^k\|_2^2-\left\langle d^k,x^{k+1}-x^k\right\rangle+\lambda\sum_{i=1}^n\left(\|D_ix^k\|_2\right)\end{aligned} \tag{4.4}$$

Combined with the concept of subgradient, the following equation is obtained

$$H(x)\geq H(x^k)+\left\langle d^k,x-x^k\right\rangle,\forall x\in R^n$$

In particular,

$$\begin{aligned}&\sum_{i=1}^n\left(\|D_ix^{k+1}\|_2\right)+c\|x^{k+1}\|_2^2-\frac{1}{\gamma}\sum_{i=1}^n\log\left(1+\gamma\|D_ix^{k+1}\|_2\right) \\ &\geq\sum_{i=1}^n\left(\|D_ix^k\|_2\right)+c\|x^k\|_2^2+\left\langle d^k,x^{k+1}-x^k\right\rangle\end{aligned} \tag{4.5}$$

Subtracting (4.4) from (4.5) and comparing it with (4.4), we have

$$E(x^k)-E(x^{k+1})\geq 0.$$

Secondly, since the sequence $\{E(x^k)\}$ is monotonically decreasing, for all $k\geq 0$, it is resulted as $E(x^k)\leq E(x^0)$. Since the function $E(x)$ is level-boundedness, then it is noted that the sequence $\{x^k\}$ is bounded.

Now, we prove that $\lim_{k\to\infty}\|x^{k+1}-x^k\|_2=0$. For the convenience of discussion, the $\|D_ix\|_2^2$ item is expanded as follows

$$\begin{aligned}\|D_ix\|_2^2&=\|D_i(x-x^k)+D_ix^k\|_2^2 \\ &=\|D_ix^k\|_2^2+\|D_i(x-x^k)\|_2^2+2(x-x^k)^TD_i^TD_ix^k \\ &\geq\|D_ix^k\|_2^2+\frac{\|(x-x^k)^TD_i^TD_ix^k\|_2^2}{\|D_ix^k\|_2^2}+2(x-x^k)^TD_i^TD_ix^k \\ &=\left\|\|D_ix^k\|_2+(x-x^k)^T\frac{D_i^TD_ix^k}{\|D_ix^k\|_2}\right\|_2^2\end{aligned} \tag{4.6}$$

It is much easier to observe from (4.6) that

$$\|D_ix\|_2-\|D_ix^k\|_2\geq(x-x^k)^T\frac{D_i^TD_ix^k}{\|D_ix^k\|_2},\forall x \tag{4.7}$$

Then, from the inequality properties of logarithmic functions ($\frac{1}{\gamma}\log(1+\gamma t)\leq t,\ \forall t\in R,\ \gamma>0$) and (4.7), it is obtained as

$$\begin{aligned}&\left(\|D_ix\|_2-\frac{1}{\gamma}\log(1+\gamma\|D_ix\|_2)\right)-\left(\|D_ix^k\|_2-\frac{1}{\gamma}\log(1+\gamma\|D_ix^k\|_2)\right) \\ &=\|D_ix\|_2-\|D_ix^k\|_2-\frac{1}{\gamma}\log\left(1+\frac{\gamma\left(\|D_ix\|_2-\|D_ix^k\|_2\right)}{1+\gamma\|D_ix^k\|_2}\right) \\ &\geq\|D_ix\|_2-\|D_ix^k\|_2-\frac{\|D_ix\|_2-\|D_ix^k\|_2}{1+\gamma\|D_ix^k\|_2} \\ &=\frac{\gamma\|D_ix^k\|_2\left(\|D_ix\|_2-\|D_ix^k\|_2\right)}{1+\gamma\|D_ix^k\|_2}\geq\frac{\gamma(x-x^k)^TD_i^TD_ix^k}{1+\gamma\|D_ix^k\|_2}\end{aligned}$$

Then, for all $x\in R^n$, and is noted as

$$\begin{aligned}H(x)&=c\|x\|_2^2+\sum_{i=1}^n\|D_ix\|_2-\Phi_\gamma(Dx) \\ &\geq c\|x\|_2^2+\sum_{i=1}^n\left(\|D_ix^k\|_2-\frac{1}{\gamma}\log(1+\gamma\|D_ix^k\|_2)+\frac{\gamma(x-x^k)^TD_i^TD_ix^k}{1+\gamma\|D_ix^k\|_2}\right) \\ &=c\|x\|_2^2+c\|x-x^k\|_2^2+2c\left\langle x^k,x-x^k\right\rangle+\sum_{i=1}^n\|D_ix\|_2 \\ &\quad-\Phi_\gamma(Dx)+\sum_{i=1}^n\frac{\gamma(x-x^k)^TD_i^TD_ix^k}{1+\gamma\|D_ix^k\|_2} \\ &=H(x^k)+\left\langle d^k,x-x^k\right\rangle+c\|x-x^k\|_2^2\end{aligned} \tag{4.8}$$

From the inequality (4.8) and the definition of (3.2), obtained as

$$\begin{aligned}E(x^{k+1})&=G(x^{k+1})-H(x^{k+1}) \\ &\leq G(x^{k+1})-\{H(x^k)+\left\langle d^k,x^{k+1}-x^k\right\rangle+c+c\|x^{k+1}-x^k\|_2^2\} \\ &=J(x^{k+1},x^k)-c\|x^{k+1}-x^k\|_2^2 \\ &\leq E(x^k)-c\|x^{k+1}-x^k\|_2^2\end{aligned} \tag{4.9}$$

Adding both sides of (4.13) from $k=0$ to ∞,

$$c\sum_{k=0}^{\infty}\| x^{k+1}-x^{k}\|_2^2\leq E(x^0)-E(x^{k+1})<\infty$$

Because $c>0$, of the above relationship and the properties of the series, it is noted that $\lim_{k\to\infty}\| x^{k+1}-x^{k}\|_2=0$.

Proposition 4.2. For any $\forall x\in R^n$, we have a property for the subgradient of $\Phi_\gamma(Dx)$,

$$\partial\Phi_\gamma(Dx)\subseteq\partial\left(\sum_{i=1}^{n}\| D_i x\|_2\right)-\partial\left(\sum_{i=1}^{n}\| D_i x\|_2-\Phi_\gamma(Dx)\right).$$

Proof. The set $D_i x=(x_{ix,}x_{iy})$ is the gradient at pixel *i*, and

$$g(x_{ix,}x_{iy})=\sqrt{x_{ix}^2+x_{iy}^2}$$

$$\phi_\gamma(\sqrt{x_{ix,}^2+x_{iy}^2})=\frac{1}{\gamma}\log(1+\gamma\sqrt{x_{ix,}^2+x_{iy}^2}),s>0\,.$$

Then we obtain

$$\begin{cases}\Phi_\gamma(Dx)=\prod_i\partial\phi_\gamma(\sqrt{x_{ix,}^2+x_{iy}^2})\\ \partial\sum_{i}^{n}(\| D_I x\|_2)=\prod_i\partial g(x_{ix},x_{iy})\\ \partial\left(\sum_{i}^{n}(\| D_I x\|_2)-\Phi_\gamma(Dx))\right)=\prod_i\partial\left(g(x_{ix},x_{iy})-\phi_\gamma(\sqrt{x_{ix,}^2+x_{iy}^2})\right).\end{cases}$$

The functions g,ϕ and $(\boldsymbol{g}\text{-}\boldsymbol{\phi})$ are discontinuous at the point (0,0). It is noted that the proof proposition 4.2 is supposed to be estimated at the point (0,0). For a detailed analysis, please refer to [28]; the proofs are omitted.

Theorem 4.2. According to Proposition 4.2, any limit point x^* of $\{x^k\}$ satisfies the weak first-order optimality condition of the $E(x)$, i.e.

$$0\in\partial\left(\sum_{i=1}^{n}\| D_i x^*\|_2\right)-\partial\left(\sum_{i=1}^{n}\| D_i x^*\|_2-\lambda\Phi_\gamma(Dx^*)\right)+A^T(Ax^*-y)$$

Proof. It follows from the Bolzano-Weierstrass theorem and Theorem 4.1 that there exists a subsequence $\{x^{k_n}\}\subset\{x^k\}$, such that $x^{k_n}\to x^*$. Then,

$$\begin{aligned}0\in{}&A^T(Ax^{k_n}-y)+2c(x^{k_n}-x^{k_n-1})\\&+\partial\left(\sum_{i=1}^{n}\| D_i x^{k_n}\|_2\right)-\lambda\sum_{i=1}^{n}(D_i^T f_i^{k_n-1}q_i^{k_n-1})\end{aligned}\qquad(4.10)$$

From the definition of f_i^k,q_i^k in (3.9) and Proposition 4.2,

$$D^T f^{k_n-1}q^{k_n-1}=\partial\left(\sum_{i=1}^{n}(\| D_i x^{k_n-1}\|_2)-\lambda\Phi_\gamma(Dx^{k_n-1})\right)$$

For $x^{k_n}\to x^*$, is obtained as

$$x^{k_n}-x^{k_n-1}\to 0,\ \ Dx^{k_n}\to Dx^*,$$

and,

$$D^T f^{k_n-1}q^{k_n-1}\to D^T f^* q^*.$$

Then,

$$0\in\partial\left(\sum_{i=1}^{n}\| D_i x^*\|_2\right)-\partial\left(\sum_{i=1}^{n}\| D_i x^*\|_2-\lambda\Phi_\gamma(Dx^*)\right)+A^T(Ax^*-y).$$

This completes the proof.

V. NUMERICAL EXPERIMENTS

This section demonstrates the numerical results to show the effectiveness of the proposed LogTV method and the comparison to traditional TV [21]. In addition, the most recent proposed nonconvex methods MCTV [12] and AtanTV [16], are also presented. All experiments are conducted using Windows 10 and MATLAB R2015a on the PC (Intel(R) Core(TM) i5-5200U CPU @ 2.20GHZ, 8.00G RAM).

In this study, the peak signal-to-noise ratio (PSNR), the relative error (RE), and the structural similarity index measurement (SSIM) are used to evaluate the quality and accuracy of image reconstruction, which are respectively defined as

$$\text{PSNR}=10\lg\left(\frac{255^2}{\| x^k-\mu_x\|_2^2}\right),\ \ \text{RE}=\frac{\| x^k-\mu_x\|_2^2}{\| x\|_2^2},$$

$$\text{SSIM}(x,x^k)=\frac{2\mu_x\cdot\mu_{x^k}+C_1(2\sigma_{xx^k}+C_2)}{({\mu_x}^2+{\mu_{x^k}}^2+C_1)({\sigma_x}^2+{\sigma_{x^k}}^2+C_2)},$$

where $\boldsymbol{x}$ represents the original MRI data, μ_x is the mean of value x,k represents the number of iterations of the algorithm, x^k is the restored image, μ_{x^k} represents the mean of x^k, σ_x^2 denotes the variance of x, $\sigma_{x^k}^2$ denotes the value x^k, σ_{xx^k} denotes the covariance of x and x^k, C_1, C_2 are stabilization parameters. Among the three quantitative evaluation index, the smaller the RE, the better the effect of model reconstruction. For the PSNR, the larger the value, the better the reconstruction effect. Moreover, the SSIM value lies in the range of [0,1], with a value closer to one indicating better structure preservation. In visual effect evaluation, the reconstruction effects of different models and the difference image between the reconstructed image and the observed image are given for each MRI observation image to compare better and analyze the results.

In Figure 3-7, five MR images are chosen, which include (Shepp Logan (256×256), Brain (256×256), Brain angiography (256×256), Shepp Logan (512×512), and Brain (512×512)). For the image reconstruction experiment, three different sample models will be used to evaluate the performance of the proposed LogTV model. Moreover, comparing the results of four reconstruction models (TV, MCTV, AtanTV, and LogTV) will be evaluated using three sampling templates (radial, Cartesian, and random sampling). In the experiments, the parameters are defined as $\lambda=0.001$, $\rho=40$, $\gamma=10$.

In Figs 3-5, the Shepp Logan (256) / Brain (256)/ Brain angiography (256) are chosen to evaluate the performance of the LogTV method. The comparison is conducted separately for the four reconstruction models (TV, MCTV, AtanTV, and LogTV) proposed above under radial, Cartesian, and random sampling. Firstly, from the visual effect, the MR images effect reconstructed by the new LogTV model is better than the other three models. Furthermore, it is obviously seen that the reconstructed images of the LogTV model are much more precise. In addition, from the specific numerical results, it is observed that the LogTV method can reconstruct Shepp Logan(256) PSNR≈45.2533, which is much higher than TV, MCTV, and AtanTV methods at least 4.6%; Brain(256) PSNR≈37.8437, Brain angiography (256) PSNR≈38.0511 are also higher than the other three methods.

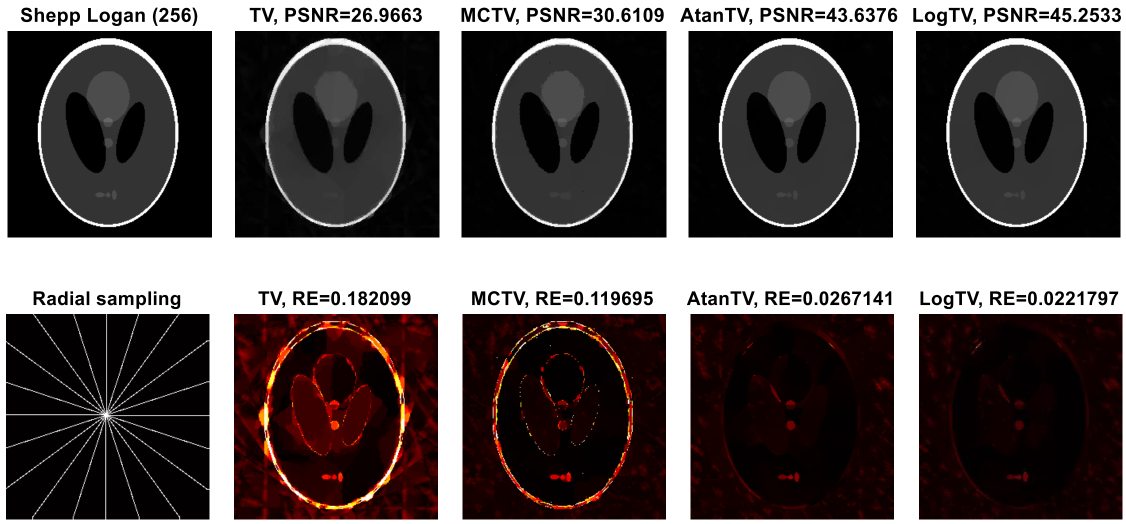

Fig.3. Reconstruction results of four methods for Shepp Logan (256) data with a radial sampling rate of 3%

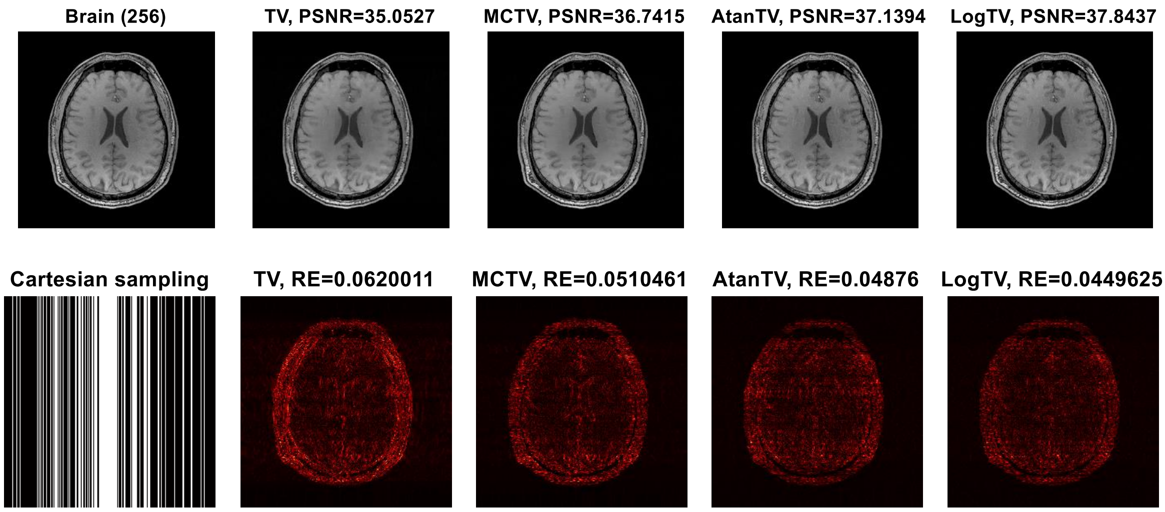

Fig.4. Reconstruction results of four methods for Brain (256) data with a Cartesian sampling rate of 34%

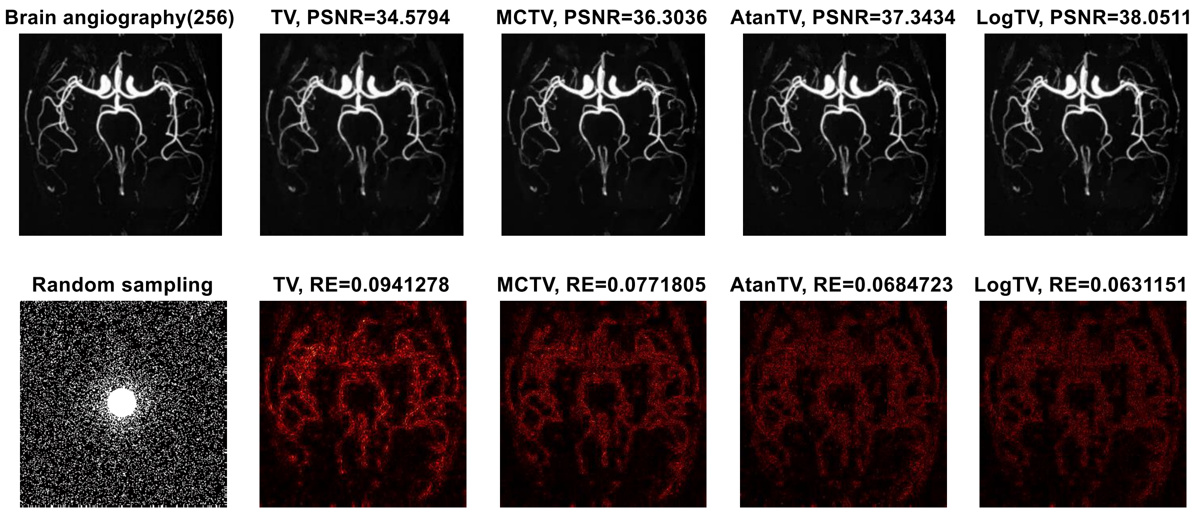

Fig.5. Reconstruction results of four methods for Brain angiography (256) data with a random sampling rate of 20%

At the same time, the RE of reconstruction with the LogTV model is observed to be very small under different sampling. For example, it is noted that the RE of Shepp Logan (256) is 0.02217, Brain (256) 's is 0.04496, and Brain angiography (256) 's is 0.06311 which all of these values showed much lower than TV, MCTV, and AtanTV. As a result, intuitively, from the reconstructed images in Figs 3-5, it is obvious that the LogTV model's reconstructed images are much more precise than others.

From the previous results combined with **Table 1**, it could be concluded as follows:

- Under the three common undersampling templates, the reconstruction results obtained by the nonconvex method are better than the traditional TV method in overall quality;
- Among SIMM, PSNR, and RE, the LogTV method proposed in this paper is superior to the other three methods.
- Both the LogTV and the traditional TV methods show good CPU time performance. In 256 data, the traditional TV method has a slight advantage, but in 512 data, the LogTV is better.
- In comparing three different nonconvex methods (MCTV, AtanTV, LogTV), the LogTV model has advantages in reconstruction quality and CPU time. The MCTV is the most time-consuming CPU method among the four methods

Without losing generality, the 512 MRI data is selected to test the new method's performance. In Figs 6-7, the test on the performance of the LogTV method on MRI data of size 512 (Shepp Logan (512) and Brain (512)) is conducted. Similarly, a comparison of the four modes (TV, MCTV, AtanTV, and LogTV) under random and radial sampling, respectively. The images with higher reconstruction accuracy through numerical experiments are obtained. The PSNR of LogTV is 73.3411 and 35.5977 under random sampling and radial sampling, which is higher than TV, MCTV, and AtanTV by 1.4% to 35%. And the RE of reconstruction with the LogTV model is also very small (0.00087/0.06948) and almost close to 0, which is lower than TV, MCTV, and AtanTV. In the residual comparison in Fig 6, we used 100 times residual to display the image and intuitively compare the differences between the four methods.

Table 1: Comparison of SIMM, PSNR, RE, and CPU time values for the four methods

Image	Template	Method	SIMM	PSNR(dB)	RE%	CPU time(s)
Shepp Logan(256)	Radial sampling	TV	0.6532	26.9663	18.21%	**6.314958**
		MCTV	0.8445	30.6109	11.97%	31.821030
		AtanTV	0.8732	43.6376	2.67%	13.338544
		LogTV	**0.9018**	**45.2533**	**2.22**%	6.748855
Brain (256)	Cartesian sampling	TV	0.8818	35.0527	6.20%	**5.102444**
		MCTV	0.9276	36.7415	5.10%	27.952286
		AtanTV	0.9273	37.1394	4.88%	12.878166
		LogTV	**0.9289**	**37.8437**	**4.50**%	5.777371
Brain angiography (256)	Random sampling	TV	0.9398	34.5794	9.41%	**5.307055**
		MCTV	0.9555	36.3036	7.72%	28.194166
		AtanTV	0.9538	37.3434	6.85%	12.741378
		LogTV	**0.9617**	**38.0511**	**6.31**%	5.464318
Shepp Logan(512)	Random sampling	TV	0.9816	54.9544	0.72%	33.535037
		MCTV	0.9856	56.2440	0.62%	209.093998
		AtanTV	0.9987	66.8811	0.18%	63.806695
		LogTV	**0.9997**	**73.3411**	**0.09**%	**32.341778**
Brain (512)	Radial sampling	TV	0.9081	34.5786	7.81%	32.152920
		MCTV	0.9294	34.0809	8.27%	209.583115
		AtanTV	0.9752	35.1145	7.35%	64.890815
		LogTV	**0.9799**	**35.5977**	**6.95**%	**31.541220**

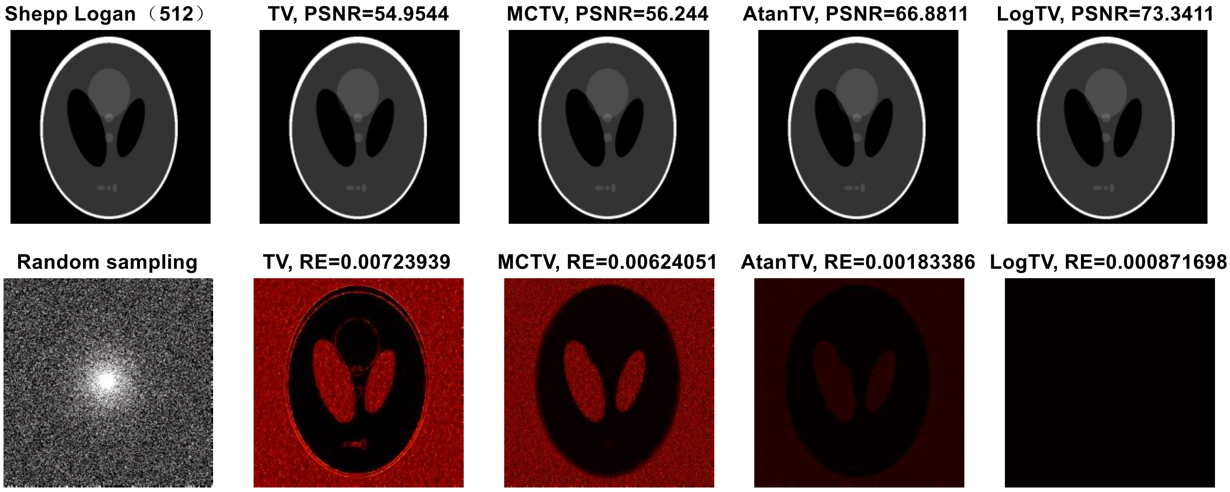

Fig.6. Reconstruction results of four methods for Shepp Logan (512) data with a random sampling rate of 30%

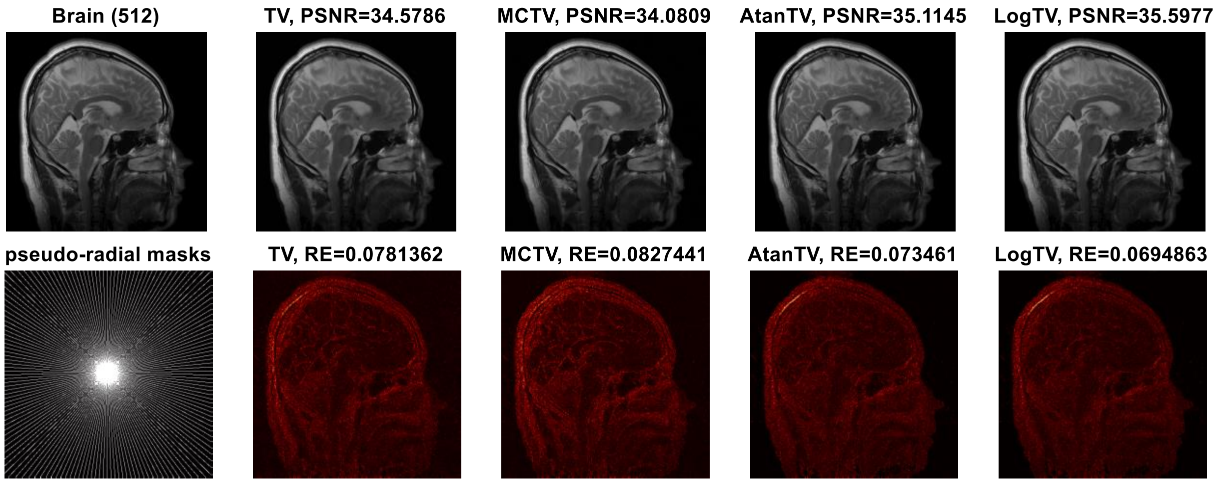

Fig.7. Reconstruction results of four methods for Brain (512) data with a pseudo-radial sampling rate of 17%

The advantages of the new model and algorithm are reflected in PSNR and RE, as well as the speed of image reconstruction and the similarity between the actual and original images. Further comparison of reconstruction results is shown in Table I. From Table I, it can be seen that the image reconstruction speed of the LogTV method is faster. For example, 512 high-dimensional image reconstruction only takes about 30 seconds, nearly 6 times faster than the MCTV method. Furthermore, images with higher PNSR and smaller RE are reconstructed at close speed compared with TV. In addition, it also can be seen that the SSIM values(0.9018, 0.9289, 0.9617, 0.9997, 0.9799) under the LogTV model all are higher and close to 1 from the simulation results, and always higher than other models in all experiments.

Figs 8-9 show the effects of the sampling rate and the number of iterations on MR image reconstruction results. As can be seen from Figs 8-9, the comparison results of the relative error values between the reconstructed model images and the original images are obtained by changing the sampling rate and the number of iterations. Under different sampling rates and different numbers of iterations, the relative error between the reconstructed image and the original image of the LogTV model is lower than that between the reconstructed image and the original image of the other two models, and the higher the sampling rate or the increasing number of iteration, the lower the relative error between the reconstructed image and the original image, which is closer to the original image in visual effect.

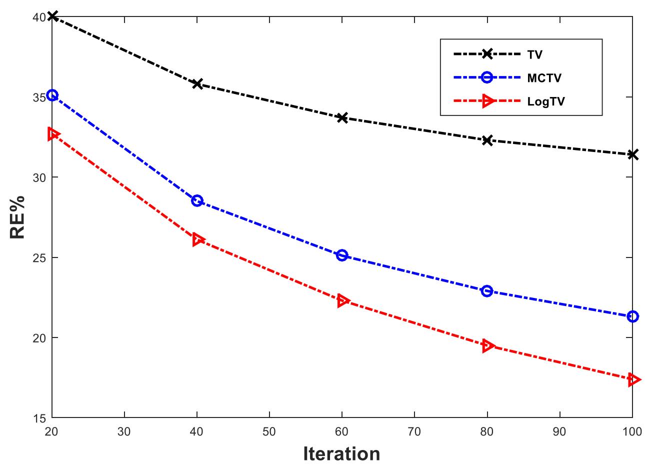

Fig.8. Comparison of RE and number of iterations on Brain (256).

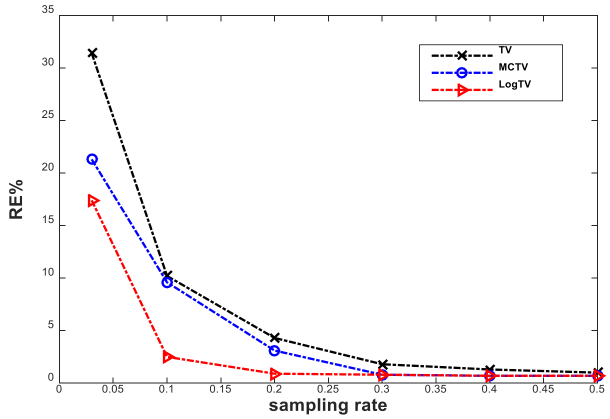

Fig.9. Comparison of RE and sampling rates on Brain (256) with different reconstruction models

The experimental results show that the LogTV model has an excellent reconstruction effect, consistent with the theoretical inference.

VI. CONCLUSION

In this paper, a nonconvex regularization model for MRI reconstruction is constructed by the logarithmic penalty function. Compared with the traditional TV model, this model can effectively improve the fitting performance of the system. In the solution of the new model, the objective function is decomposed with the help of the convex difference technique, and then the ADMM algorithm is used to solve the sub-problem. Theoretical analysis and numerical experiments demonstrate the convergence and effectiveness of the algorithm, respectively. In the future, the LogTV model should be tested for more sparse systems such as video processing, dynamic MRI, etc. In addition, in recent years, with the deep integration of nonconvex models in deep learning, machine learning, and other fields, how to apply the new methods proposed in this paper to these fields is the focus of later research.

REFERENCES

[1] Fengfei Ma, Suzhen Lin, Feng Liu, Lifang Wang, and Dafang Li, "Semantic-contrast Generative Adversarial Network Based Highly Undersampled MRI Reconstruction," Computer Science, vol. 48, no.4, pp169 -173, 2021

[2] David L. Donoho, "Compressed Sensing," IEEE Transactions on Information Theory, vol. 52, no.4, pp1289 -1306, 2006

[3] Emmanuel J. Candès, Justin Romberg, and Terence Tao, "Robust Uncertainty Principles: Exact Signal Reconstruction from Highly Incomplete Frequency Information," IEEE Transactions on Information Theory, vol. 52, no.2, pp489 -509, 2006

[4] Michael Lustig, David L. Donoho, and John M. Pauly, "Sparse MRI: the Application of Compressed Sensing for Rapid MR Imaging," Magnetic Resonance in Medicine, vol. 58, no.6, pp1182 -1195, 2007

[5] Michael Lustig, David L. Donoho, Juan M. Santos, and John M. Pauly, "Compressed Sensing MRI," IEEE Signal Processing Magazine, vol. 25, no.2, pp72 -82, 2008

[6] Leonid I. Rudin, Stanley Osher, and Emad Fatemi, "Nonlinear Total Variation Based Noise Removal Algorithms," D: N Physica on Linear Phenomena, vol. 60 no.1, pp.259 -268, 1992

[7] Jianping Zhang, Ke Chen, and Bo Yu, "An Iterative Lagrange Multiplier Method for Constrained Total-Variation-Based Image Denoising," SIAM Journal on Numerical Analysis, vol. 50, no.3, pp983 -1003, 2012

[8] Yiping Xu, "A New Algorithm for Total Variation Based Image Denoising," Acta Mathematicae Applicate Sinica, English Series, vol. 28, no.4, pp721 -730, 2012

[9] Yilun Wang, Junfeng Yang, Wotao Yin, and Yin Zhang, "A New Alternating Minimization Algorithm for Total Variation Image Reconstruction," SIAM Journal on Imaging Sciences, vol.1, no.4, pp248 -272, 2008

[10] Tibshirani, Robert, "Regression Shrinkage and Selection via the Lasso," Journal of the Royal Statistical Society, Series B, vol, 58, no.1, pp267 -288, 1996

[11] Yi Shen, Song Li, "Restricted p–Isometry Property and Its Application for Nonconvex Compressive Sensing," Advances in Computational Mathematics, vol. 37, no.3, pp441 -452, 2012.

[12] Yilin Liu, Huiqian Du, Zexian Wang, and Wenbo, Mei, "Convex MR Brain Image Reconstruction via Non-Convex Total Variation Minimization," International Journal of Imaging Systems and Technology, vol. 28, no.4, pp246 -253, 2018

[13] Marui Shen, Jincheng Li, Tao Zhang, and Jian Zou, "Magnetic Resonance Imaging Reconstruction via Non-Convex Total Variation Regularization," International Journal of Imaging Systems and Technology, vol. 31, no.1, pp412 -424, 2021

[14] Mehranian Abolfazl, Hamidreza Saligheh Rad, Arman Rahmim, Mohammad Reza Ay, and Habib Zaidi, "Smoothly Clipped Absolute Deviation (SCAD) Regularization for Compressed Sensing MRI Using an Augmented Lagrangian Scheme," IEEE Nuclear Science Symposiwn and Medical Imaging Conference Record, pp3646 -3653, 2012

[15] Zhijun Luo, Zhibin Zhu, and Benxin Zhang, "An SCADTV Nonconvex Regularization Approach for Magnetic Resonance Imaging," IAENG International Journal of Computer Science, vol. 48, no.4, pp1013 -1020, 2021

[16] Zhijun Luo, Zhibin Zhu, and Benxin Zhang, "An AtanTV Nonconvex Regularization Model for MRI Reconstruction," Journal of Sensors, vol. 2022, 2022.

[17] Benxin Zhang, Guopu Zhu, Zhibin Zhu, "A TV-log Nonconvex Approach for Image Deblurring with Impulsive Noise," Signal Processing, vol. 174, no.9, pp1 -15, 2020

[18] Chunfeng Wang, Yaping Deng, and Xiaodi Wu, "A Convexity Method for Linear Multiplicative Programming," IAENG International Journal of Applied Mathematics, vol. 52, no.1, pp66-70, 2022

[19] Fessler, Jeffrey A, "Optimization Methods For Magnetic Resonance Image Reconstruction: Key Models And Optimization Algorithms," IEEE Signal Processing Magazine, vol. 37, no.1, pp33 -40, 2020

[20] Stephen Boyd, Neal Parikh, Eric Chu, Borja Peleato, "Distributed Optimization and Statistical Learning via the Alternating Direction Method of Multipliers," Foundations and Trends in Machine Learning, vol. 3, no.1, pp1-122, 2011

[21] Junfeng Yang, Yin Zhang, and Wotao. Yin, "A Fast Alternating Direction Method For TVL1-L2 Signal Reconstruction from Partial Fourier Data," IEEE Journal of Selected Topics in Signal Processing, vol. 4, no.2, pp288-297, 2010

[22] Yan Yang, Jian Sun, Huibin Liu, Zongben Xu, "Deep ADMM-Net for Compressive Sensing MRI," Advances in Neural Information Processing Systems, vol. 29, 10 -18, 2016

[23] Benxin Zhang, Zhibin Zhu, "Linearized Proximal Alternating Direction Method of Multipliers for Parallel Magnetic Resonance Imaging," IEEE/CAA Journal of Automatica Sinica, vol. 4, no.4, pp763-769, 2016

[24] Bingsheng, Feng Ma, Xiaming Yuan," Optimally Linearizing the Alternating Direction Method of Multipliers for Convex Programming," Computational Optimization and Applications, vol. 75, no.2, pp361-388, 2020

[25] Yan Gu, Nobuo Yamashita, "An Alternating Direction Method of Multipliers with the BFGS Update for Structured Convex Quadratic Optimization," Computational and Applied Mathematics, vol. 40, no.3, pp1 -27, 2021

[26] Emmanuel J. Candès, Michael B. Wakin, and Stephen P. Boyd, "Enhancing Sparsity by Reweighted L1 Minimization," Journal of Fourier Analysis & Applications, vol. 14, no.5, pp877 -905, 2008

[27] Ivan Selesnick, Masoud Farshchian, "Sparse Signal Approximation via Nonseparable Regularization," IEEE Transactions on Signal Processing, vol. 65, no.10, pp2561 -2575, 2017

[28] Yuli Sun, Hao Chen, Jinxu Tao, and Lin Lei, "Computed Tomography Image Reconstruction from Few Views via Log-Norm Total Variation Minimization," Digital Signal Processing, vol. 88, pp172-181, 2019